Article

A ground reaction force model of speed skating based on non-contact measurement system

Step 1

1 day

Motion capture experiments
Use markerless motion capture systems to obtain the kinematic data

Step 2

2 hours

Data pre-processing
Smooth kinematic data

Step 3

1 hour

Stroke Detection
Split the data into several strokes based on the kinematic data

Step 4

8 hours

Data processing and force estimation
Get the estimated Ground Reaction Force data from the OAM model

Qihang Zhu, Chunxin Yang, Peng Ke, Han Yang, Ping Hong

p.ke@buaa.edu.cn

Highlights

Achieve the estimation of GRF based on the non-contact measurement approach

Build a GRF model with optimizing variables estimating forces intelligently

Propose a new simple stroke identification method for speed skating

Emphasize the double-feet-supporting phase, improving motion pattern accuracy
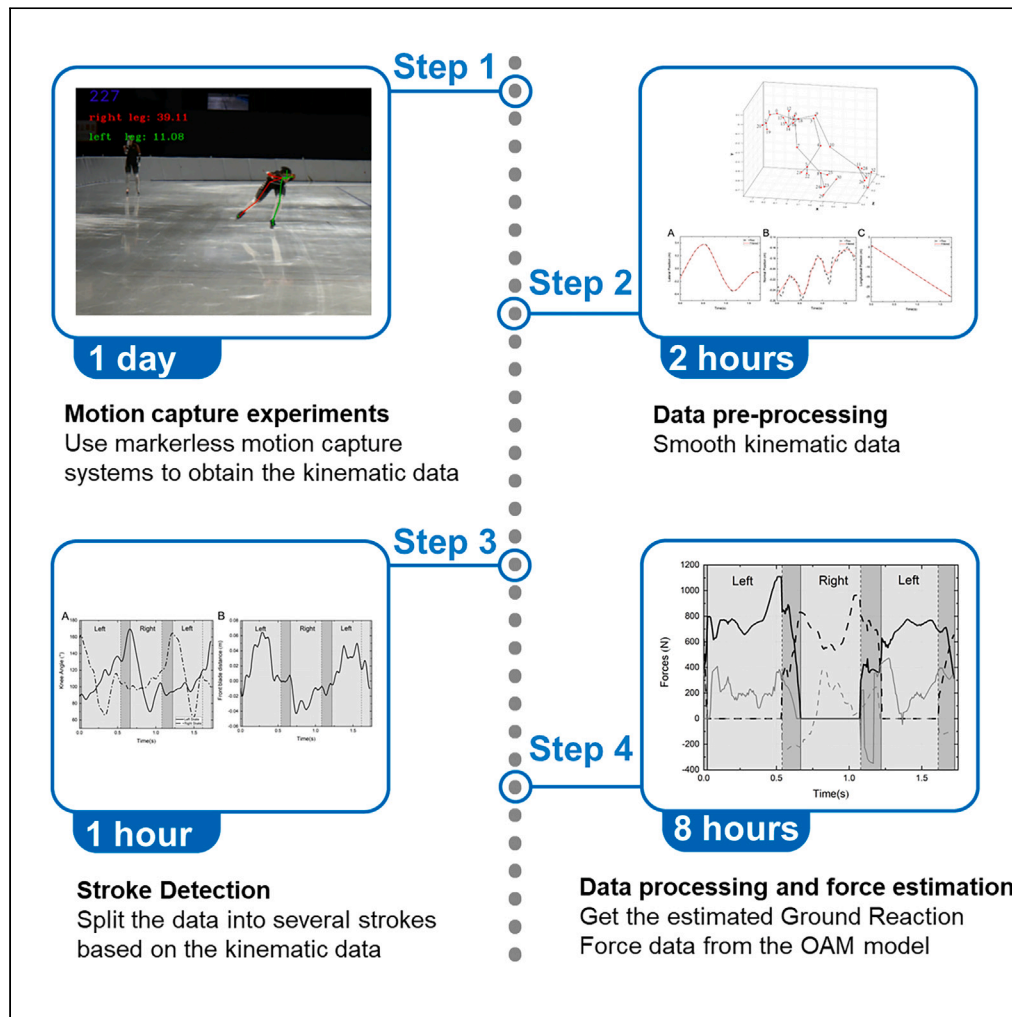
Article

A ground reaction force model of speed skating based on non-contact measurement system

Qihang Zhu,[1] Chunxin Yang,[2] Peng Ke,[3,6,*] Han Yang,[4] and Ping Hong[5]

SUMMARY

Accurate collection and analysis of ground reaction force (GRF) data are crucial for optimizing the technical movements of speed skaters; however, it has been a challenge for the limitations of experimental equipment and application scenarios. Therefore, we proposed a novel approach for estimating GRF based on kinematics obtained from markerless video tracking systems and achieved low errors compared with the experimental data. Our method allows for further biomechanical analysis, including muscle force and power, during speed skating competitions.

INTRODUCTION

Biomechanical simulation is a powerful tool for identifying factors that affect athletic performance and providing recommendations for sports training (Koning et al.[1]; Van Ingen Schenau et al.[2]). Developing accurate musculoskeletal models requires precise kinematic and kinetic analysis of motion capture data and ground reaction force (GRF) data obtained from various sensors.

Motion capture data can be obtained using vision-based systems or inertial sensors. Inertial sensors, such as IMUs containing accelerometers, gyroscopes, and magnetometers, allow for the orientation of the subject to be solved by double integration of the measured acceleration (Bonnet et al.[3]; Seel T et al.[4]). Vision-based systems, such as optoelectronic motion capture systems, use multiple high-speed cameras to capture the movements of the entire body. Active and passive markers can be used in vision-based systems, with the former having its own light source (Richards et al.[5]) and the latter reflecting light from the camera back to the sensors. Whereas active markers require additional cables and power, passive markers can be used in larger environments. In addition, indoor global positioning systems (IGPSs), which are based on receivers attached to the object, can be used for markerless tracking (van der Kruk et al.[6]).

Image processing systems (IPSs) based on optical cameras and computer vision algorithms are a significant advantage for sports research, as they allow for markerless tracking (Liu et al.[7]; Klous et al.[8]). This makes them a useful tool for experiments in sports research, particularly in competition arenas where sensors attached to the object may be limiting.

GRF measurement is a crucial technique in sports science research, as researchers rely on it to assess the factors that affect athletes' performance. Previous studies have demonstrated that GRF features play a significant role in determining skating efficiency and speed (Yuki et al.[9]; van der Kruk et al.[10]). However, it can be challenging to gather biomechanical data on speed skaters during competitions due to the expense and complexity of force measurement systems.

To address this challenge, we propose a non-contact measurement technique that can be used to acquire data for speed-skating-related biomechanical simulation models. Such models have been developed by researchers such as Fintelman et al.[11] and van der Kruk et al.,[12] who sought to mimic the forces experienced by speed skaters. However, their studies assumed that the predicted force was the total combined force and did not account for the double stance phase. This approach results in a combined force acting on both legs, rather than split forces on each leg, which can obscure important information about shifts in the center of mass.

In this study, we present a novel method for constructing a three-dimensional optimization-algorithm speed skating model (OAM) to predict both the GRF and motion of speed skaters. Our approach is based on kinematic data obtained from non-contact experiments using IPS, which allows for unobtrusive measurement of athlete movement during competitions and other high-stakes scenarios. Importantly, our model accounts for the splitting force between the left and right legs during the double stance phase, resulting in more accurate predictions of skater.

[1]School of Aeronautic Science and Engineering, Beihang University, Beijing 100191, China
[2]School of Aeronautic Science and Engineering, Beihang University, Beijing 100191, China
[3]School of Transportation Science and Engineering, Beihang University, Beijing 100191, China
[4]School of Aeronautic Science and Engineering, Beihang University, Beijing 100191, China
[5]Beijing Sport University, Beijing 100084, China
[6]Lead contact
*Correspondence: p.ke@buaa.edu.cn
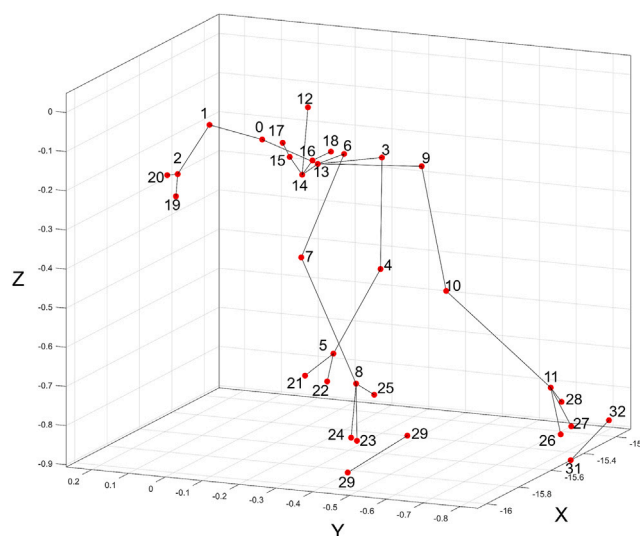https://doi.org/10.1016/j.isci.2023.108513

Figure 1. Experimental data
Schematic diagram of the locations of the 33 interest points.

RESULTS AND DISCUSSION

The data input for the OAM model was obtained from video capture experiments via two cameras at an ice rink in Beijing, 2021, where the raw data were the location of human body points identified by a video-based algorithm, with a total of 33 interest points, collected at a frequency of 150 Hz, as shown in Figure 1 and Table 1. The data were collected for two participants for four experiments in total, as shown in Table 2, in addition to the model verification results. In this section, the experimental data and estimation results of Participant A Trial 1 were presented in details as a case study (See Figures 2, 3, 4, 5, 6, and 7; Table 3).

Table 1. Definition of the 33 interest points in experiments

Number	Body position	Number	Body position
0	r-shoulder	17	r-ear
1	r-elbow	18	l-ear
2	r-wrist	19	r-thumb
3	l-shoulder	20	r-little finger
4	l-elbow	21	l-thumb
5	l-wrist	22	l-little finger
6	r-hip	23	r-big toe
7	r-knee	24	r-little toe
8	r-ankle	25	r-heel
9	r-hip	26	l-big toe
10	l-knee	27	l-little toe
11	l-ankle	28	l-heel
12	head	29	r-blade front
13	neck	30	r-blade back
14	nose	31	l-blade front
15	r-eye	32	l-blade back
16	l-eye		

The front texts "r" and "l" indicate the right and left side of the body, respectively.

Table 2. Residuals and errors of the model—UO for unoptimized; O for optimized

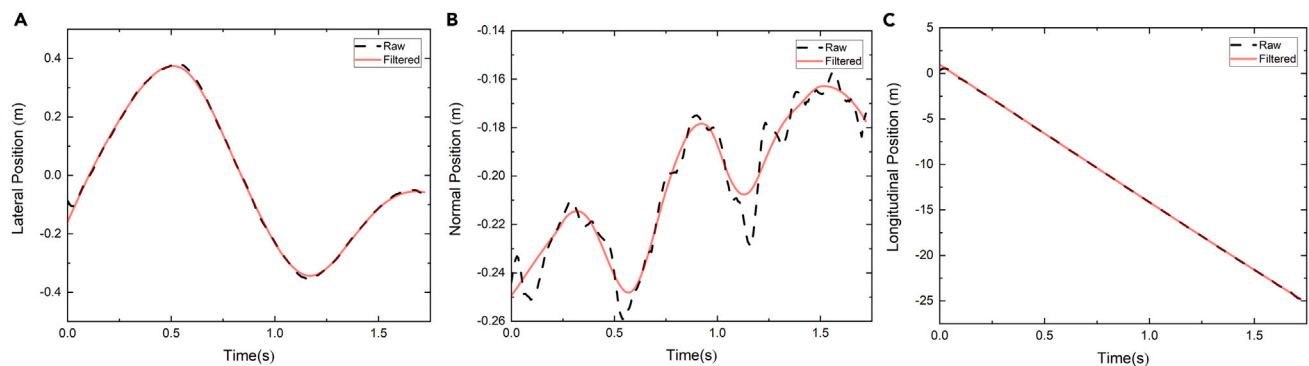| Participant			A		B					
m		(kg)	80		78					
l		(m)	1.8		1.78					
h		(m)	0		0		0		0	
μ			0.000		0.000		0.000		0.000	
Trial			1		1		2		3	
Stroke			3		2		3		1	
Method			UO	O	UO	O	UO	O	UO	O
Residuals	Rx	(m)	0.283	0.011	0.541	7.26e-03	0.608	0.118	0.284	3.78e-03
	Ry	(m)	0.436	1.20e-03	1.597	2.66e-03	1.761	8.77e-03	0.597	4.88e-04
	Rz	(m)	0.418	0.33	1.673	1.628	0.206	7.13e-02	0.193	5.29e-02
	Rdx	(m/s)	0.671	0.054	0.670	4.23e-02	0.619	0.422	0.768	4.72e-02
	Rdy	(m/s)	1.171	0.014	0.769	2.28e-02	0.858	7.31e-02	0.581	9.86e-03
	Rdz	(m/s)	0.655	0.475	2.753	2.723	0.486	0.249	0.518	0.139
Errors	Ex	%	0.133	0.0004	38.579	0.016	31.036	3.881	159.670	0.005
	Ey	%	0.120	0.0003	20.598	0.020	19.923	1.366	23.215	0.008
	Ez	%	0.001	0.0003	1.276	1.214	0.013	0.001	0.029	0.002
	Edx	%	0.221	0.002	85.736	0.202	19.437	15.890	37.087	0.669
	Edy	%	0.209	0.003	35.155	0.309	28.013	2.778	32.665	0.177
	Edz	%	0.003	0.001	6.844	6.753	0.200	0.049	0.119	0.010
J		%	11.48	0.121	31.37	1.42	16.37	3.99	42.13	0.145
$(J_{NO} - J_O)/J_{NO}$		%		98.9		95.5		75.6		99.7

The specific experimental methods, the established model, and the associated schematics and tables (Figures 8, 9, 10, 11, 12, 13, 14, and 15; Tables 4, 5, and 6) are described in the STAR Methods.

Measured data

Position and pose

As illustrated in Figure 2, the lateral and vertical motion patterns of the body's center of mass (COM) follow a sine/cosine signal, with the COM moving toward the swing leg. Although the range of variation in the vertical COM position amplitude is small, being about 0.1 m in three strokes, the magnitude of the air drag area tends to remain stable. Notably, the z-direction motion follows a nearly linear pattern.

The results of the skate pose are presented in Figure 3. As illustrated in Figure 3A for Participant A Trial 1, the steer angle of the landing leg remained between 0 and 10°. When the angle noticeably increased (indicated by the dark area in the figure), it signaled that the landing leg

Figure 2. Experimental data measurement of the COM position—raw versus filtered
(A) Lateral position, (B) normal position, (C) longitudinal position. Data were calculated based on 15-segment rigid body assumption—Participant A Trial 1.
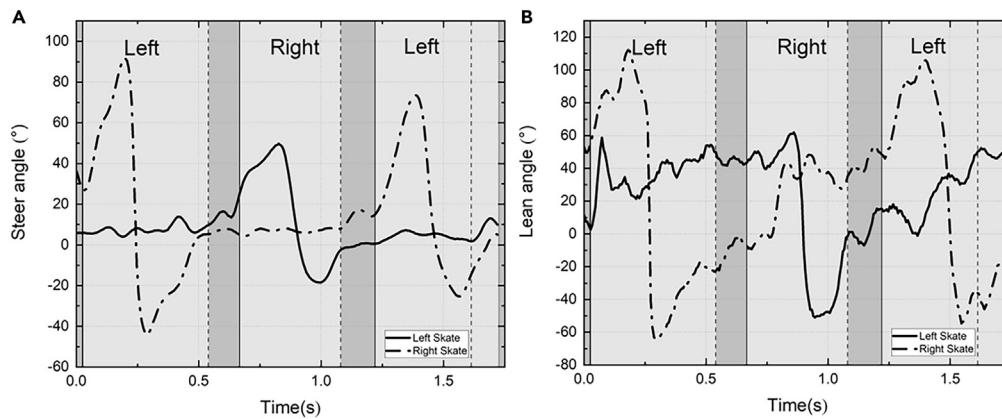
Figure 3. Experimental data measurement of two pose angles

(A) Steer angle; (B) lean angle. The solid line indicates the left foot, and the dotted line indicates the right foot—Participant A Trial 1.
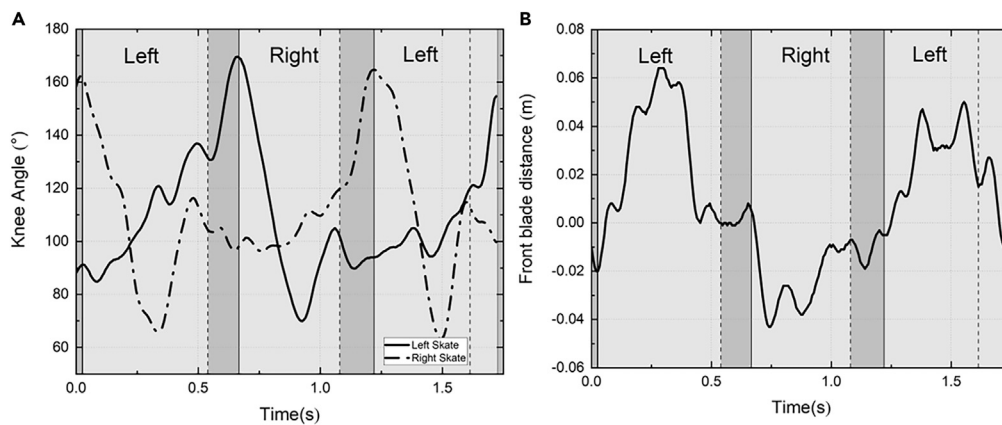

Figure 4. Input data for stroke detection

(A) Knee angle, denoted by the angle between thigh and calf.

(B) Distance between front points of two skates. Solid and dashed lines indicate left and right foot, respectively. The vertical dashed and solid lines indicate the time points of foot-on and foot-off, respectively. The dark area between them indicates the double stance phase, and the text indicates which skate is active (on the ice). Same below—Participant A Trial 1.
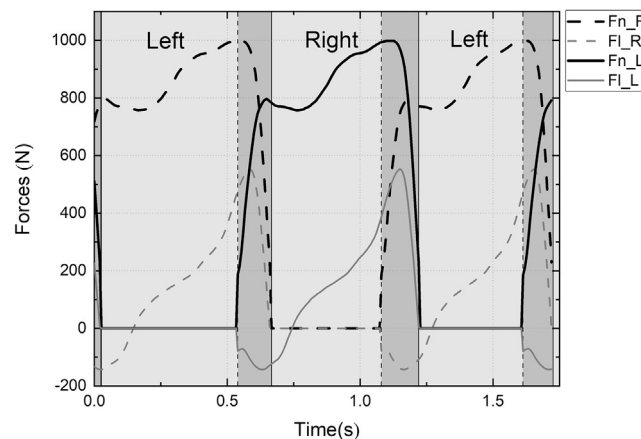

Figure 5. Unoptimized forces

The statistical results of GRFs obtained from reference (van der Kruk et al.[10])—Participant A Trial1. For lateral forces, the direction is negative toward the medial direction. In the figure legend, lowercase letters "n" and "l" denote normal and lateral directions, respectively, and capital letters "L" and "R" denote left and right legs, respectively. For example, the abbreviation "Fn_R" stands for the normal forces in the right leg.
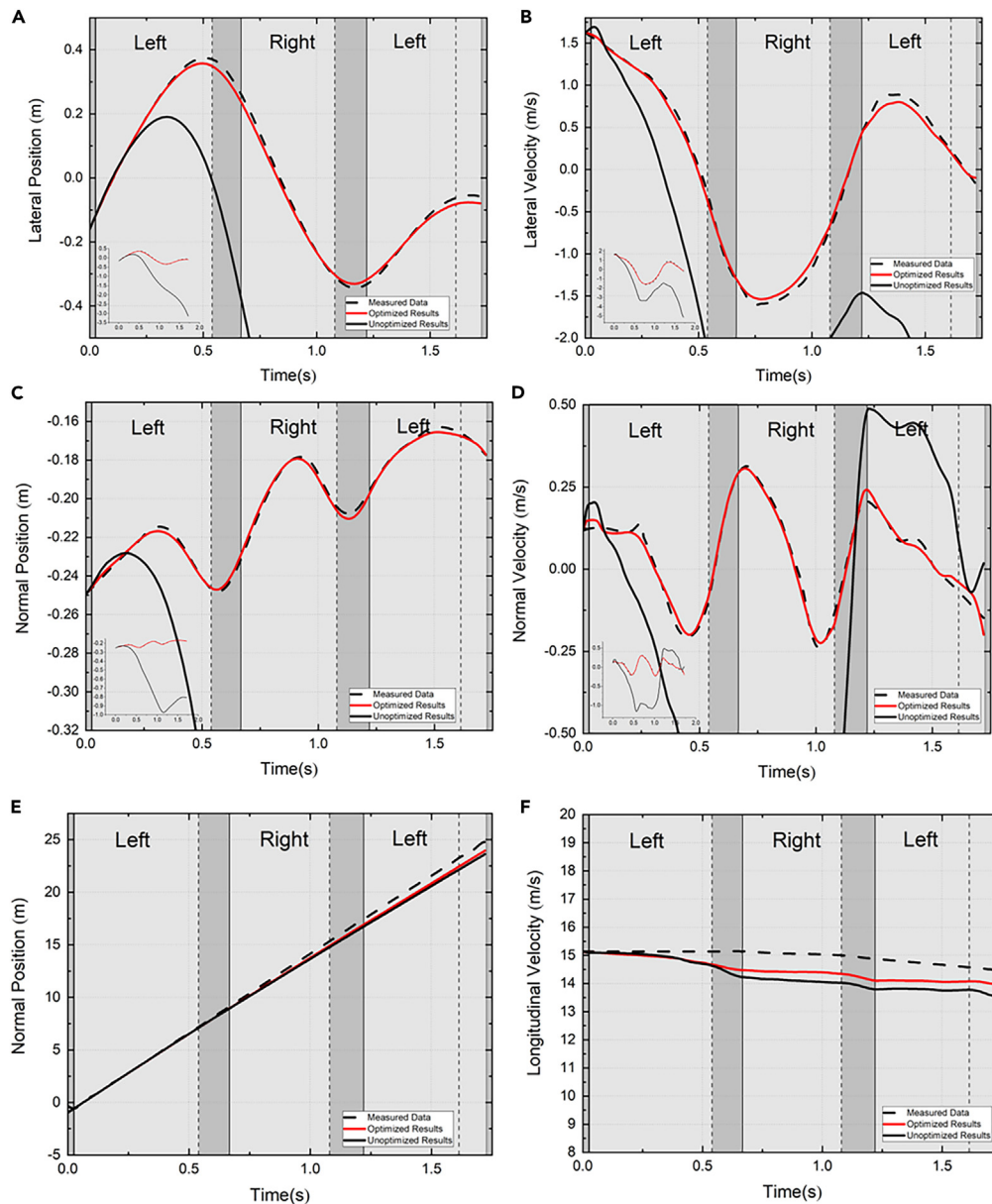
Figure 6. Results of COM position with two methods versus experimental data—Participant A Trial 1
(A)Lateral position; (B) lateral velocity; (C) vertical position; (D) vertical velocity; (E) longitudinal position; (F) longitudinal velocity. The red solid line indicates the result of the optimized algorithm, the black solid line indicates the result of the unoptimized method, and the black dashed line indicates the result of the experimental measurement data.

was about to leave the ground, and the other leg would initiate the landing. Similarly, Figure 3B shows that the lean angle tended to increase while the landing leg was in the swing phase, and the overall level increased gradually from −20° to 50°, which was consistent with the statistics reported by van der Kruk et al.[10]

Stroke detection

Four extreme values of the knee angle were found for Participant A Trial as shown in Figure 3A. The presence of these values indicates that there were three strokes in total during the observed time duration. Similarly, as depicted in Figure 3B, the distance between the two blade front points at the end of each stroke was almost zero (less than 0.01 m), and the distance between points was closest to zero during the double stance phase (highlighted in dark in the figure), which was in sharp contrast to the inter-stroke distance.
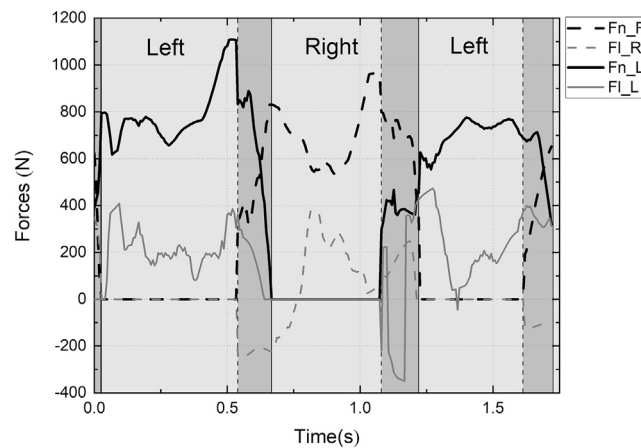
Figure 7. Ground reaction forces predicted by the optimization algorithm model—Participant A Trial 1

Table 3. Optimized parameters in genetic algorithm—Participant A Trial 1

	Skate	Force	$t_1(\%T)$	$F_1(\%BW)$	$t_2(\%T)$	$F_2(\%BW)$	Scale
Stroke 1	Left	FN	23.9	95.69	79.2	114.28	1.06
		FL	5.8	1.11	85.4	60.51	0.88
Stroke 2	Right	FN	19.9	87.15	95.0	110.17	0.98
		FL	16.9	−13.17	95.0	55.48	0.93
Stroke 3	Left	FN	13.6	92.43	79.1	120.41	0.75
		FL	5.0	1.07	80.4	52.15	1.09

The units of t_1 and t_2 denote the percent time points in a stroke. The expressions of these two variables are the same, but independent for forces in different directions, and the units of F_1 and F_2 denote the percent forces of the body weight gravity.

We utilized the stroke detection method to obtain a set of unoptimized real-time GRF data, based on the statistical data of GRF. The forces during the three strokes were found to follow the same pattern, as illustrated in Figure 5. The vertical coordinate of the graph represents forces normalized according to body weight. The values are determined based on the foot-on and foot-off time points and scaled according to the duration of the stroke. Notably, the normal and lateral forces were set to zero when the foot was off the ground.

Model data

According to Figure 6, the results obtained using the simple approach exhibited some similarity in the predicted motion trend along the x and z axes, although their accuracy was deemed insufficient when compared with the measured data. In addition, there were notable calculation errors with respect to the displacement velocity along the y axis, particularly concerning the speed of deviation during the double stance phase. This was primarily attributed to an excessive normal force in this phase, and taking into account that displacement and velocity are integral equations of acceleration, they are susceptible to cumulative effects from the initial time point, which increases the magnitude of
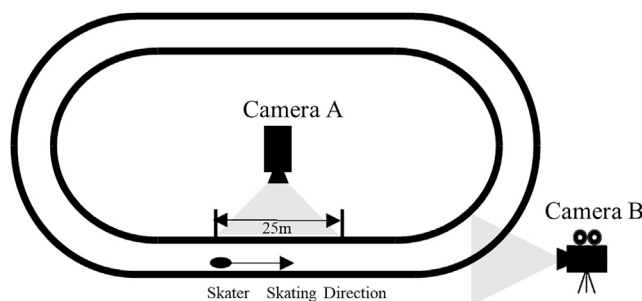

Figure 8. The placements of cameras in the ice rink

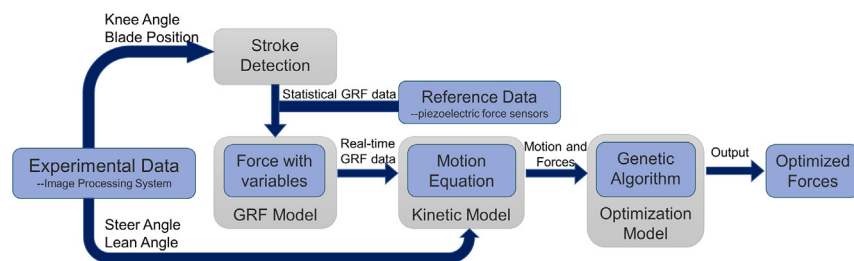**Figure 9. The calibration for frontal viewing screens**

Figure 10. Flowchart of the OAM model

calculation deviations. The primary limitation of this method was the fixed force characteristics that could not accommodate individual variations among athletes and stroke patterns. To address this issue, we introduced characteristic variables t, F, $Scale$ to capture the diversity of force characteristics of different athletes during a stroke. We optimized these variables using a genetic algorithm and provided the results in Table 3. Although good optimization results were realized, optimization along the z axis was not significant. This was due to the initial velocity of the skater being relatively high and calculated acceleration being of smaller magnitude as a result of the skate angle, which reduced the component of the GRF in the Z-direction, leading to slight differences between results obtained from different methods with fixed initial velocity.
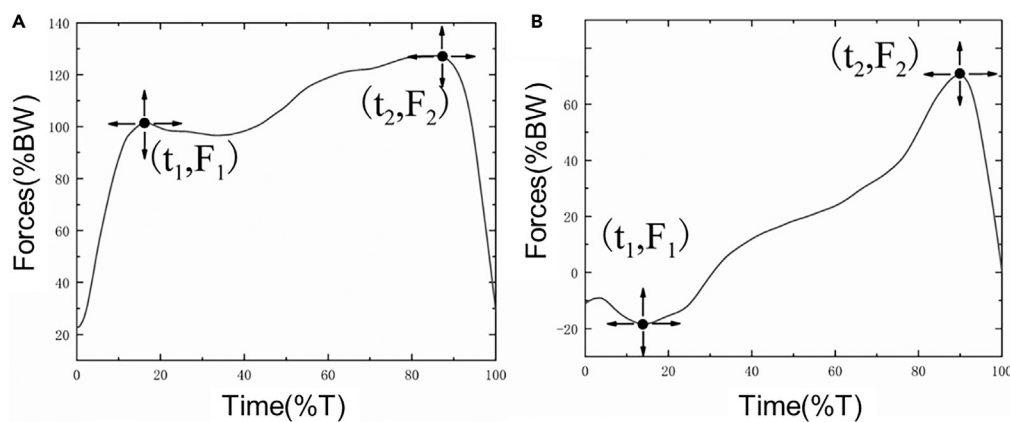

Figure 11. The location of variables in the original force curve with fixed patterns
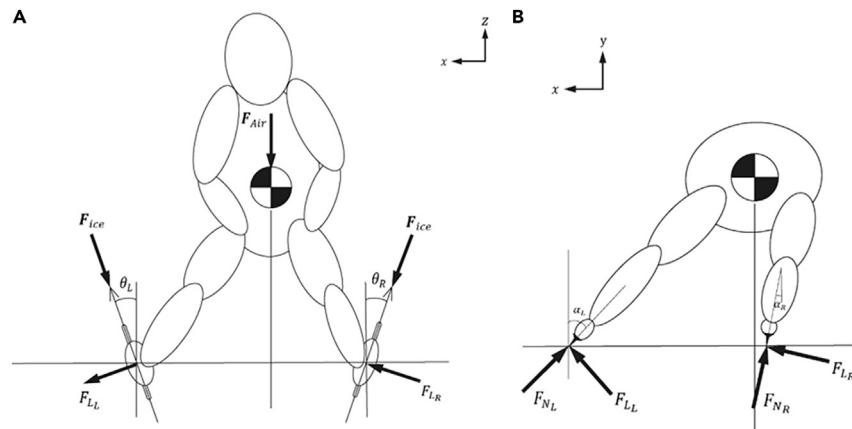(A) Normal force; (B) lateral force.

Figure 12. Speed skating model
(A) Top view of the skater; (B) rear view of the skater. The skater is considered as one single mass with three freedoms. The position of this mass is located at the COM of 15 segments (Hanavan et al.[14]), which is indicated in the torso.

According to Figure 7, there are three complete strokes in total, and combining the results shown in Figure 3, it is easily observed that the signs of the lateral force are almost consistent with the lean angle. In the second stroke, the curve of the lateral force was the most satisfactory; however, the results in the third one had an obvious discontinuity, due to the sign changing of the lean angle. Although the lean angle at this transformation time was positive, we rechecked the experimental data and found that shank lean angle at the same time was still negative, so the left leg did not start to push off the ice, and the real time point to push off was around 1.35 s when the lateral force and the lean angle were both almost zero. In general, this phenomenon was caused by the sign inconsistency between the shank and the foot lean angle in the experiment measurement results.

According to Table 2, the GRF estimation model proposed in this paper had certain generality for analyzing the speed skating motion in the straight, although the number of strokes analyzed here was no more than three. Because the skating process in the track could be divided into three phases—start, straights and curves—skating athletes would apply different techniques in different phases, and especially for the high-level ones, the coordination in each stroke keeps highly consistent in a certain phase, showing their technical stability. Besides, this paper focused on the start phase in the straight, which is the most important phase for short-distance races; generally it consists of a few strikes. Therefore, the proposed estimation model has enough generality for analyzing available experimental data captured by current experiment equipment. And analyses with more strokes could be carried out if capturing range could be extended or the amount of experiment was added.

Conclusion

In this paper, a novel approach is presented for estimating and optimizing the ground reaction force (GRF) in speed skating using stroke identification and genetic algorithm optimization methods, all relying on non-contact vision-based systems. The optimization model was
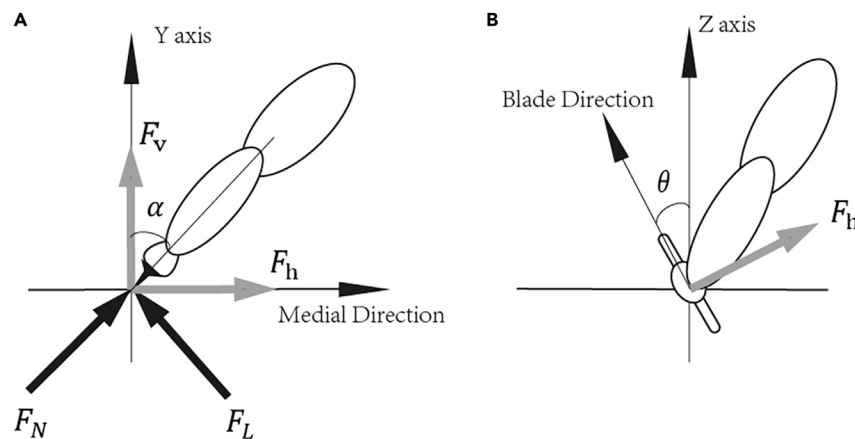

Figure 13. Skate angle diagram
(A) Lean angle, rear view of the left skate, positive in the medial position.
(B) Steer angle, top view of the left skate, positive in the opposite of the medial position. F_N is positive in the vertical direction, and F_L is positive when lean angle is positive.
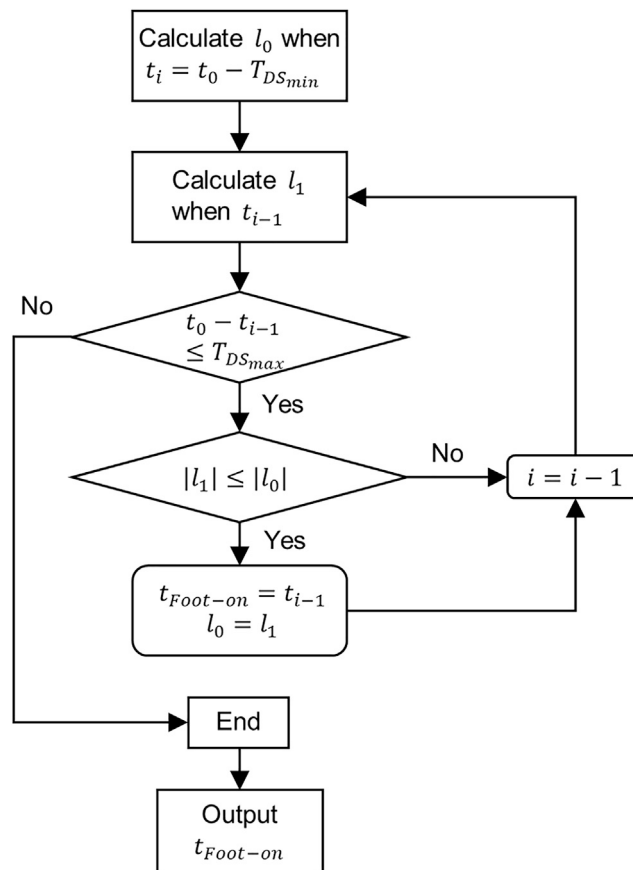
Figure 14. Flowchart of the stoke detection method

successfully applied to different athletes and various numbers of strokes, with a minimum total error of 0.12% and a maximum error of 4% compared with experimental data. The optimized model also achieved a 99.7% maximum error reduction compared with the unoptimized results.

Unlike previous research in speed skating biomechanics, this model considers the double stance phase, incorporates variables to be optimized in the GRF model, and utilizes stroke identification to predict the GRF. Furthermore, the model provides motion simulation analysis based on non-contact measurement data. This non-contact approach allows for biomechanical analysis under race conditions without interfering with the athletes and can provide valuable insights for technical and tactical improvements and physical strength training. Additionally, the model can optimize force characteristic parameters and offer technical advice to athletes for maximizing their forward speed.

Limitations of the study

In this study, measuring ground reaction forces (GRF) accurately during a real speed skating race can be challenging due to several factors, like dynamic nature, equipment limitations, environmental conditions, athlete variability, etc. It makes the problem worse if we need to obtain the data via the equipment that do not affect athletes' performance or impede their movements.

Additionally, the model simplifies the skater's body to a mass point model, overlooking the rotational energy of each joint and the energy loss resulting from force transmission between body segments. Consequently, the estimated GRF from the model may slightly exceed the actual GRF.

To enhance the accuracy of the model in the future, it is suggested to incorporate more degrees of freedom, such as masses for the upper body, swing leg, or standing leg. This would provide a more comprehensive representation of the skater's biomechanics and likely improve the estimation of the GRF. The model still needs to be further validated by experimental force measurements using unobtrusive high-quality sensors, even though the simulated motion matches the experimental data well now.

STAR★METHODS

Detailed methods are provided in the online version of this paper and include the following:
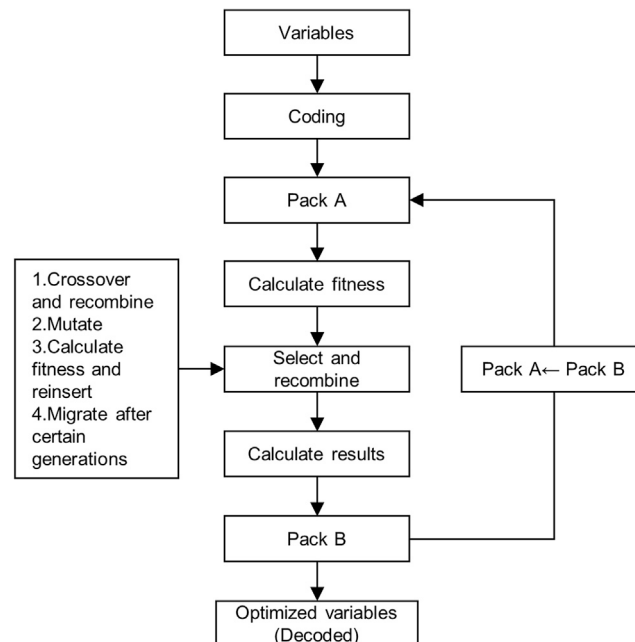
- KEY RESOURCES TABLE

Figure 15. Flowchart of genetic algorithm optimization

- RESOURCE AVAILABILITY
  - Lead contact
  - Materials availability
  - Data and code availability
- EXPERIMENTAL MODEL AND STUDY PARTICIPANT DETAILS
- METHOD DETAILS
  - Ground reaction force model
  - Kinetic model
  - Kinematic analysis and stroke detection
  - Genetic Algorithm Model
  - Model verification
- QUANTIFICATION AND STATISTICAL ANALYSIS

SUPPLEMENTAL INFORMATION

Supplemental information can be found online at https://doi.org/10.1016/j.isci.2023.108513.

Table 4. Force parameter settings							
Force	t_1 (%T)	F_1 (%BW)	t_2 (%T)	F_2 (%BW)	Scale	R_{min} (%BW)	R_{max} (%BW)
Normal Forces	[5,25]	[80,120]	[75,95]	[107,147]	[0.7,1.3]	−20	20
Lateral Forces	[5,25]	[−38,0)	[75,95]	[50,90]	[0.7,1.3]	−20	40

The units of t_1 and t_2 denote the percent time points in a stroke. The expressions of these two variables are the same, but independent for forces in different directions, and the units of F_1 and F_2 denote the percent forces of the body weight gravity.

t_1, F_1, t_2, F_2, Scale are the parameters to be optimized in the genetic algorithm; R_{min} and R_{max} are the constraint settings in the LSE approach.

Table 5. The number, mass, and expression for calculating COM of the 15 body segments

Number	Segment	Mass (kg) -A	Mass (kg) -B	COM position
1	Head	6.014	5.850	P_{14}
2	Torso	11.991	11.347	$0.5 * (P_{13} + 0.5*(P_6 + P_9)) P_6 + P_9)) P_{13} + 0.5*$
3	Pelvis	18.882	17.798	$0.5 * (P_6 + P_9) - (0, 0.1477, 0)$
4	Thigh-right	10.131	9.539	$P_6 + 0.42*(P_7 - P_6)$
5	Thigh-left	10.131	9.539	$P_9 + 0.42*(P_{10} - P_9)$
6	Shank-right	3.198	2.962	$P_7 + 0.45*(P_8 - P_7)$
7	Shank-left	3.198	2.962	$P_{10} + 0.45*(P_{11} - P_{10})$
8	Foot-right	0.977	0.925	$1/3*(P_{23} + P_{24} + P_{25})$
9	Foot-left	0.977	0.925	$1/3*(P_{26} + P_{27} + P_{28})$
10	Upper arm-right	2.017	1.893	$0.5 * (P_0 + P_1)$
11	Upper arm-left	2.017	1.893	$0.5 * (P_3 + P_4)$
12	Forearm-right	1.105	0.987	$0.5 * (P_1 + P_2)$
13	Forearm-left	1.105	0.987	$0.5 * (P_4 + P_5)$
14	Hand-right	0.512	0.484	P_2
15	Hand-left	0.512	0.484	P_5

P_i represents the 3-D position of the i-th number in Table 1. A for participant A; B for participant B. Regarding the calculation of COM position, part of them (No.3–7) take a reference from the muscle skeleton model in Opensim, and rest of them are in the centroid of lines, triangles, or squares.

AUTHOR CONTRIBUTIONS

DECLARATION OF INTERESTS

The authors declare no competing interests.

Table 6. The values and definition of the basic parameters of the genetic algorithm

Name	Value	Meaning of name
NVAR	10*S	Number of variables
GGAP	0.9	Gap
XOVR	1	Crossover ratio
MUTR = 1/NVAR	1/NVAR	Mutation ratio
MAXGEN	300	Max number of generations
INSR	0.9	Insertion ratio
SUBPOP	20	Number of subpopulations
MIGR	0.2	Migration ratio
MIGGEN	20	Migration generation
NIND	300	Number of individuals
MAXTOR	1e-4	The min tolerance of iterations

REFERENCES

1. de Koning, J., and Schenau, G.J. (2008). Performance-Determining Factors in Speed Skating. In Biomechanics in Sports, pp. 232–246.

2. van Ingen Schenau, G.J., de Koning, J.J., and de Groot, G. (1990). A simulation of speed skating performances based on a power equation. Med. Sci. Sports Exerc. *22*, 718–728.

3. Bonnet, V., Joukov, V., Kulic, D., Fraisse, P., Ramdani, N., and Venture, G. (2016). Monitoring of Hip and Knee Joint Angles Using a Single Inertial Measurement Unit During Lower Limb Rehabilitation. IEEE Sens. J. *16*, 1557–1564.

4. Seel, T., Raisch, J., and Schauer, T. (2014). IMU-Based Joint Angle Measurement for Gait Analysis. Sensors *14*, 6891–6909.

5. Richards, J.G. (1999). The measurement of human motion: A comparison of commercially available systems. Hum. Mov. Sci. *18*, 589–602.

6. Van der Kruk, E. (2013). Modelling and Measuring 3D Movements of a Speed Skater. http://resolver.tudelft.nl/uuid:2a54e547-0a5a-468b-be80-a41a656cacc1.

7. Liu, G., Tang, X., Cheng, H.D., Huang, J., and Liu, J. (2009). A novel approach for tracking high speed skaters in sports using a panning camera. Pattern Recogn. *42*, 2922–2935.

8. Klous, M., Müller, E., and Schwameder, H. (2010). Collecting kinematic data on a ski/snowboard track with panning, tilting, and zooming cameras: Is there sufficient accuracy for a biomechanical analysis? J. Sports Sci. *28*, 1345–1353.

9. Yuki, M., Ae, M., and Fujii, N. (1996). BLADE REACTION FORCES IN SPEED SKATING. Biomechanisms *13*, 41–51.

10. van der Kruk, E., den Braver, O., Schwab, A.L., van der Helm, F.C.T., and Veeger, H.E.J. (2016). Wireless instrumented klapskates for long-track speed skating. Sports Eng. *19*, 273–281.

11. Fintelman, D.M., Braver, O., and Schwab, A. (2011). A simple 2-dimensional model of speed skating which mimics observed forces and motions. In Multibody Dynamics, J.C. Samin and P. Fisette, eds., pp. 1–20. https://api.semanticscholar.org/CorpusID:1964080.

12. van der Kruk, E., Veeger, H.E.J., van der Helm, F.C.T., and Schwab, A.L. (2017). Design and verification of a simple 3D dynamic model of speed skating which mimics observed forces and motions. J. Biomech. *64*, 93–102.

13. Cabrera, D., Ruina, A., and Kleshnev, V. (2006). A simple 1+ dimensional model of rowing mimics observed forces and motions. Hum. Mov. Sci. *25*, 192–220.

14. Hanavan, E.P. (1964). A Mathematical Model of the Human Body (Aerospace Medical Research Laboratories, Aerospace Medical Division, Air Force Systems Command).

15. van Ingen Schenau, G.J. (1982). The influence of air friction in speed skating. J. Biomech. *15*, 449–458.

16. Van Ingen Schenau, G.J. (1981). A Power Balance Applied to Speed Skating.

17. Tomita, Y., Iizuka, T., Irisawa, K., and Imura, S. (2021). Detection of Movement Events of Long-Track Speed Skating Using Wearable Inertial Sensors. Sensors *21*, 3649.

18. Clark, K.P., and Weyand, P.G. (2014). Are running speeds maximized with simple-spring stance mechanics? J. Appl. Physiol. *117*, 604–615.

STAR★METHODS

KEY RESOURCES TABLE

REAGENT or RESOURCE	SOURCE	IDENTIFIER
Deposited data		
statistical data of Ground Reaction Forces during speed skating	van der Kruk et al.[10]	https://doi.org/10.1007/s12283-016-0208-8

RESOURCE AVAILABILITY

Lead contact

Further information and requests for resources and reagents should be directed to and will be fulfilled by the lead contact, Peng Ke (p.ke@buaa.edu.cn).

Materials availability

This study did not generate new unique reagents.

Data and code availability

- The deposited data in key resources table and other data reported in this paper will be shared by the lead contact upon request.
- This paper does not report original codes.
- Any additional information required to reanalyze the data reported in this paper is available from the lead contact upon request.

EXPERIMENTAL MODEL AND STUDY PARTICIPANT DETAILS

This study conducted video capture experiments via two cameras at an ice rink in Beijing, 2021. The placement of the camera adopts the popular scheme at present, guided by the professional experts. As shown in Figure 8, there are two cameras in total, the side one is located on the central axis of the straight, and the front one is located directly in front of the track.

We used two high-performance ZCam cameras, which has been modified by us to support simultaneous high-frame rate high-quality filming. And in this experiment, we adopted 150Hz non-zoom filming.

In addition, in order to ensure the accuracy of the camera measurement results, we performed the calibration of the camera parameters before the test (shown in Figure 9), which is a commonly used method in AI pose recognition, which can ensure the accuracy of the model calculation results in this paper.

The data was collected for two male participants from Chinese National Speed Skating Team for four experiments in total, as shown in Table 2.

METHOD DETAILS

The research concept of this paper is visually depicted in Figure 10. First, we establish a Ground Reaction Force (GRF) model by considering the force characteristics and referencing statistical outcomes from the literature, utilizing piezoelectric force sensors to improve the accuracy.

Next, we develop a mechanics model for speed skating that incorporates the steer angle (θ, °) and lean angle (α, °) based on the analysis of experiment data. These angles are used as inputs in the model.

The experimental data undergoes preprocessing to obtain the necessary input data. Then, employing a stroke detection approach using the knee angle and blade position as input, virtual periodic GRF data is transformed into real-time data and integrated into the kinetic model.

Lastly, the genetic algorithm model is utilized for optimization of the GRF parameters. This optimization process ensures that the estimated GRF aligns with the observed experimental data.

Overall, this methodology enables us to accurately estimate the GRF by integrating various models and experimental data. This approach has the potential to enhance the understanding of speed skating mechanics and contribute to sports training and performance optimization.

Ground reaction force model

During the skating stroke, the GRF on the athlete undergoes distinct changes. Initially, there is a sharp increase in GRF at the moment of initial touchdown due to the impulse generated. Subsequently, the normal force component continues to increase as the athlete's muscle force is exerted, while the lateral force component increases in response to the athlete's lean angle. Finally, as the leg begins to lift off the ice, the force rapidly diminishes.

In a study conducted by Van der Kruk et al.[10], experiments were conducted on a group of skaters to measure both normal and lateral forces. The researchers found that the pattern of the normalized force closely resembles the shape observed in the same pattern. Building

upon these findings, this study develops a parametric GRF model that incorporates the characteristics of the GRF and experimental data. To optimize the model parameters, an intelligent algorithm is employed to estimate the GRF accurately.

By integrating the identified GRF characteristics and the experimental data, this study aims to advance our understanding of the forces exerted during the skating stroke. The parametric model, optimized through the intelligent algorithm, provides a valuable tool for predicting and analyzing GRF in speed skating.

Unoptimized forces

The unoptimized forces were utilized as input in the approach after stroke detection (details below), using the statistical data of normal and lateral forces from van der Kruk et al.'s literature[10] as the benchmark or starting point for optimization.

Forces with variables

The functional expression for GRF with variables can be expressed as

$$F = f(g(Scale, mg, t_1, F_1, t_2, F_2), \{R_{min}, R_{max}\}, \{t_{on1}, t_{off1}, \cdots t_{oni}, t_{offi}, \cdots\}) \qquad \text{(Equation 1)}$$

Equation 1 can be divided into three parts. The left part in f function represents the expression of virtual periodic forces, which variables are to be optimized in Genetic Algorithm Model. The middle part describes the boundary conditions of the constraints. Meanwhile, the right part represents a set of parameters (i indicate the i-th stroke), determined by the motion's characteristics using the method discussed in stroke detection, to convert the virtual ground reaction forces into real-time.

The g function is determined based on the periodic GRF supported by at least two variables. Figure 11 demonstrates that the two local maxima force points (t_1, F_1) and (t_2, F_2) are the characteristic variables for normal force, while the minimum (t_1, F_1) and maximum (t_2, F_2) force points are the characteristic variables for lateral force. These variables divide the curve into three segments, and the force curve is scaled based on the movement of these variables. Finally, a global variable $Scale$ is added to scale the whole force curve. So periodic GRF can be expressed by:

$$F_P = g(Scale, mg, t_1, F_1, t_2, F_2) = Scale * mg * h(t_1, F_1, t_2, F_2) \qquad \text{(Equation 2)}$$

Based on Equation 2, upper and lower bounds are defined for the constraints in the least squares error (LSE) approach:

$$Scale * h(t_1, F_1, t_2, F_2) + R_{min} \leq F_p/mg \leq Scale * h(t_1, F_1, t_2, F_2) + R_{max} \qquad \text{(Equation 3)}$$

In this paper, the conditions of normal and lateral force are set as shown in Table 4.

In this part, we built the GRF model with variables. Some of them are known parameters (e.g. mg, R_{min}, R_{max}) or can be determined by the stroke detection method and the rest of them are to be optimized by the genetic algorithm.

Kinetic model

Model description

A simplified speed skating model is presented in Figure 12, which is based on the following assumptions

(1) The skater is represented as a single mass with three degrees of freedom
(2) the rotational motion between the joints of the body, such as that of the legs and upper arms, is not considered.
(3) The air resistance in the X and Y directions is neglected since the velocity of the air relative to the skater in these two directions is low.
(4) The moment of body rotation caused by the force arm is ignored, and all forces act directly on the center of mass (COM) of the whole body.
(5) Since the GRF measurement is basically done under foot local coordinate system, inequality between the foot rotation angle and shank rotation angle would not influence on the determination of GRF.

To execute the model, the motion of the center of mass of the body and the steer angle θ (subscripts indicate the left and right legs respectively, same below) as well as the lean angle α of the skates are utilized as inputs.

The equations of motion in terms of generalized coordinates according to Newton's law are then described by

$$\mathbf{M} \cdot \begin{bmatrix} \ddot{x} \\ \ddot{y} \\ \ddot{z} \end{bmatrix} = T_{blade} \cdot F - F_{ice} - F_{Air} - G \qquad \text{(Equation 4)}$$

where $\mathbf{M}$ represents the mass-inertia matrix (kg), T_{blade} the coefficient matrix of GRF , F the external force(N)of the GRF on the object, F_{ice} the frictional force(N) on the ice surface, F_{Air} the air drag(N),G the gravity(N) of the skater, and x, y, z the lateral, normal, and longitudinal positions(m) of the center of mass, respectively.

$\mathbf{M}$ is found by

$$\mathbf{M} = \begin{bmatrix} m & 0 & 0 \\ 0 & m & 0 \\ 0 & 0 & m \end{bmatrix}$$

(Equation 5)

where m represents the mass (kg) of the skater.

Indeed, it is important to acknowledge that the simplification of the model used in this study may introduce errors in the calculations.

For instance, the model does not account for the velocity oscillation during the stroke, which arises from the momentum exchange between the swinging leg and the upper body. This exchange of momentum can influence the forces experienced by the athlete during the stroke. By not considering this effect, the model may not fully capture the complexity of the actual forces involved.

Additionally, the model overlooks the contribution of arm movement and joint rotation during the skating stroke. Although these factors may have some impact on the forces experienced by the athlete, the study suggests that their influence is not as significant as the momentum exchange between the swing leg and upper body. (van der Kruk et al.[12]).

While these simplifications may introduce some degree of error, it is important to weigh these limitations against the benefits of having a parametric GRF model that can still provide valuable insights and predictions. Further research can explore more comprehensive models that take into account these neglected factors in order to improve the accuracy of the calculations.

Ground reaction force

As shown in Figure 12, the four components of the GRF in the local skate coordinate are expressed as

$$F = \begin{bmatrix} F_{N_L} & F_{L_L} & F_{N_R} & F_{L_R} \end{bmatrix}^T$$

(Equation 6)

T_{blade} is found by

$$T_{blade} = \begin{bmatrix} -\cos\theta_L \cdot \sin\alpha_L & \cos\theta_L \cdot \cos\alpha_L & -\cos\theta_R \cdot \sin\alpha_R & \cos\theta_R \cdot \cos\alpha_R \\ \cos\alpha_L & \sin\alpha_L & \cos\alpha_R & \sin\alpha_R \\ \sin\theta_L \cdot \sin\alpha_L & -\sin\theta_L \cdot \cos\alpha_L & -\sin\theta_R \cdot \sin\alpha_R & \sin\theta_R \cdot \cos\alpha_R \end{bmatrix}$$

(Equation 7)

The definition of the angle is shown in Figure 13.

Ice friction

The expression for the friction on the ice surface is

$$F_{ice} = -\mu \begin{bmatrix} \sin\theta_L \\ 0 \\ \cos\theta_L \end{bmatrix} \cdot \begin{bmatrix} 1 & 0 \end{bmatrix} \cdot \begin{bmatrix} F_{N_L} \\ F_{L_L} \end{bmatrix} - \mu \begin{bmatrix} -\sin\theta_R \\ 0 \\ \cos\theta_R \end{bmatrix} \cdot \begin{bmatrix} 1 & 0 \end{bmatrix} \cdot \begin{bmatrix} F_{N_R} \\ F_{L_R} \end{bmatrix}$$

$$= -\mu \begin{bmatrix} \sin\theta_L & 0 & -\sin\theta_R & 0 \\ 0 & 0 & 0 & 0 \\ \cos\theta_L & 0 & \cos\theta_R & 0 \end{bmatrix} \cdot \begin{bmatrix} F_{N_L} \\ F_{L_L} \\ F_{N_R} \\ F_{L_R} \end{bmatrix}$$

(Equation 8)

which is simplified as $F_{ice} = T_{ice} \cdot F$, where μ is the coefficient of ice surface friction.

Air drag

The air drag is obtained according to the empirical equation in the literature (van Ingen Schenau et al.[15]), which is simplified to the following functional representation

$$F_{Air} = F(v, \theta_1, \theta_0, m, l, h)$$

(Equation 9)

where v represents the velocity(m/s) of the air with respect to the skater, θ_1 the trunk angle (°), θ_0 the knee angle (°), m、l the mass(kg) and height(m) of the skater, respectively, and h is the altitude (m) at which it is located.

Kinematic analysis and stroke detection

The experimental data are the 3-D positions identified by the video-based algorithm, with a total of 33 interest points of location information, as shown in Figure 1 and Table 1.

Kinematic analysis-position and pose

By using the inertial mass parameters and the geometric parameters of the experimental subject (obtained in pre-experiments), the human body is simplified to a 15-segment rigid body (Hanavan et al.[14]), and the COM positions of the body segments are calculated by:

$$COM = \frac{\sum_{i=1}^{15} m_i * D_i}{\sum_{i=1}^{15} m_i} \qquad \text{(Equation 10)}$$

where i represents the number of the body segment, m_i, D_i represent the mass and COM position of the i-th body segment, respectively, as shown in Table 5.

According to Equation 10 and Table 5, COM of the body for participant A was obtained (See Figure 2). The results are filtered appropriately (Robust Loess Method).

Besides position, pose information is obtained by geometric calculations (See Figure 3). The steer angle can be calculated by $P_{29} \sim P_{32}$. And the skate plane is orientated according to $P_{23} \sim P_{25}$ (left) and $P_{26} \sim P_{28}$ (right), from which the lean angle is derived (See supplemental information).

Stroke Detection

In speed skating, the athlete generates forward thrust by executing sideward strokes that follow a fixed cycle pattern, particularly for experienced athletes. The strokes comprise three main phases: the glide phase, the push-off phase, and the re-position phase (Van Ingen Schenau et al.[16]). During the double stance phase, when one leg is just beginning to skate while the other leg completes a stroke, both legs are on the ice. Frequent stroking leads to greater forward propulsion, resulting in a shorter double stance phase (Tomita et al.[17]; Clark et al.[18].). The strong cyclical pattern in speed skating facilitates identifying and analyzing data in a cyclical manner (Tomita et al.[17]; Cabrera et al.[13]).

Previous studies on GRF estimation (Fintelman et al.[11]; Kruk et al.[12]) considered the time points of foot-on and foot-off together for simplicity, disregarding the duration of the double stance phase. In this study, the foot-on/off time was identified using a stroke detection method explained later. For speed skating stroke detection, the kinematic analysis obtained the skate's knee angle. To determine the starting time point (foot-on), Tomita et al.[17] combined the filtered data of foot acceleration along with the extreme value of the knee angle to determine the ending time point (foot-off). In this paper, accelerometers were unavailable, so the stroke's starting and ending points in Equation 1 were determined by the ice skate's position.

In theory, both blade front points should lie on the same horizontal plane during the double stance phase, implying that the Y-directional distance between P_{29} and P_{31} is zero. However, the unevenness of the ice surface and image processing errors make this value non-zero. Therefore, the foot-on time point is considered as the closest Y-directional distance between the two blade front points during a specific time frame. Finally, combining the knee angle and relative ice blade positions determined the foot-on and foot-off time points, as shown in Figure 14. The maximum and minimum duration of the double stance phase are represented by $T_{DS_{max}}$ and $T_{DS_{min}}$, respectively. Generally, skating speed and stroke frequency are positively correlated. Therefore, this paper calculates $T_{DS_{min}} = 1/15$ s and $T_{DS_{max}} = 1/5$ s based on this relationship considering that this range should be narrowed as the speed increases.

Genetic Algorithm Model

The focus of the genetic algorithm is to optimize the characteristic parameters of the GRF model by using the experimental kinematic data as reference. In reality, while the skating process has a pattern and the GRF of each cycle follows a statistical rule, randomness and variability also accompany the process. Hence, the force generated cannot be predicted or described using a fixed empirical force curve. Thus, the algorithm should introduce and optimize suitable variables to improve the accuracy of the model prediction. Besides the genetic algorithm model approach, this section introduces a simple approach without optimization and compares it with the former. Moreover, the calculation results of this method are not dependent on the experimental results. Thus, even if the fit is not satisfactory, the accuracy of the speed skating model can be indirectly confirmed if the trend is approximated.

Simple approach without optimization

This approach takes the initial unoptimized forces as the input.

According to Equations 4, 5, 6, 7, 8, and 9, the motion equation can be expressed as

$$M \cdot a = T_{blade}(\theta, \alpha) \cdot F - T_{ice}(\mu, \theta, \alpha) \cdot F - F_{air}(v, \theta_1, \theta_0, m, l, h) - G \qquad \text{(Equation 11)}$$

where F represents the ground reaction force, μ, m, l, h the basic parameters, $\theta, \alpha, \theta_1, \theta_0$ the input parameters obtained from the kinematic analysis of the experimental data, and $v = \int a dt$. Therefore, if there is a predicted GRF result $\overline{F}$, the acceleration a can be solved so that further integration can be done to predict the velocity and position of the body.

According to Equation 10, it is obtained by

$$a = M^{-1} \cdot ((T_{blade}(\theta, \alpha) - T_{ice}(\mu, \theta, \alpha)) \cdot \overline{F} - F_{air}(v, \theta_1, \theta_0, m, l, h) - G) \qquad \text{(Equation 12)}$$

In this section, the initial unoptimized forces (as shown in Table 4) are already available, and by combining them with Equation 3, the acceleration and body displacement can be obtained. Since the force's magnitude relies on the stroke detection outcome, i.e., the knee angle and the distance between two skates, it is independent of the body position and velocity acquired through experimental measurements.

Optimized approach with genetic algorithm

While the ground reaction force of athletes exhibits certain characteristics, as shown by van der Kruk et al.,[10] subtle differences exist between athletes and strokes for each athlete. These differences lead to significant variations in the curve characteristics between strokes and result in errors between the results of the Simple Approach and the experimental outcomes. Consequently, we introduce characteristic variables for the ground reaction force.

In this study, we introduce variables to represent the diversity of force patterns. However, determining the best combination of variable values for the actual situation is unknown. Hence, we introduce five variables for both normal and lateral forces in each stroke (See Table 4) to be optimized using the genetic algorithm. Optimization is based on errors between the OAM model and experimental results. Figure 15 provides a detailed demonstration of the process.

Number of variables is expressed as $5 * 2 * S$, where S represents the number of strokes, the range of these 10 variables for each stroke is shown in Table 4.

The basic parameters of the algorithm are shown in Table 6.

According to Equation 11, if the desired acceleration a_d (calculated from experimental data) is known, the required GRF F can be found.

However, according to the experimental data, the acceleration in three directions, lateral, vertical and longitudinal, the desired acceleration a_d can be obtained, which means that there are three equations, but F has a total of four unknowns for the normal and lateral forces in the left and right legs, respectively. Therefore, the boundary obtained from Equation 3 is introduced as a constraint and the force X_d is solved by the LSE method.

Target.

$$\min \frac{1}{2} \|AX - b\|^2 \qquad \text{(Equation 13)}$$

where $A = T_{blade} - T_{ice}, X = F = \begin{bmatrix} F_{N_L} & F_{L_L} & F_{N_R} & F_{L_R} \end{bmatrix}^T, b = F_{air} + M \cdot a_d + G$.

Constraint.

$$\begin{cases} Scale * h(t_1, F_1, t_2, F_2) + R_{min} \le F_p/mg \le Scale * h(t_1, F_1, t_2, F_2) + R_{max} \\ F = 0, \text{when the foot is off the ice} \end{cases} \qquad \text{(Equation 14)}$$

where $Scale$、t_1、F_1、t_2、F_2 are the parameters to be optimized in the genetic algorithm, R_{min}、R_{max} are the constraint settings in the LSE method, and the normal and lateral forces are taken as zero-setting constraints when the foot is off the ice according to the results of stroke detection.

The LSE solution is found as the GRF according to the expected acceleration a_d, and then the COM position of the model is calculated, which is used as the input for the next fitness calculating.

Substituting the solved force X_d into Equation 12 yields:

$$a_c = M^{-1} \cdot ((T_{blade}(\theta, \alpha) - T_{ice}(\mu, \theta, \alpha)) \cdot X_d - F_{air}(v, \theta_1, \theta_0, m, l, h) - G) \qquad \text{(Equation 15)}$$

where a_c represents the acceleration calculated from X_d, which is integrated to obtain the motion of the body COM position of the model：

$$\begin{cases} V_C = \int a_c dt + V_0 \\ P_C = \iint a_c dt^2 + P_0 \end{cases} \qquad \text{(Equation 16)}$$

where V_0, P_0 are the initial velocity and initial position of the body COM at the initial moment state obtained from the experiment.

The error between the experimental data and the model results is calculated by (Cabrera et al.[13]):

$$E\left(y_j\right) = \frac{1}{N}\sum_{i=1}^{N}\frac{\left(\tilde{y}_{ij} - y_{ij}\right)^2}{\overline{y}_j^2} \tag{Equation 17}$$

where $\tilde{y}_{ij}$ is the simulated value of a variable, y_{ij} the measured value of a variable, $\overline{y}_j$ the characteristic value of the variable, and N is the number of samples.

Taking the sum of the errors of the positions in the three directions as the fitness valuation:

$$\text{Fitness} = E(x) + E(y) + E(z) \tag{Equation 18}$$

where x, y, z denote the lateral, normal and longitudinal positions, respectively, the characteristic values of which are taken as the difference between the maximum and minimum values of them. For the genetic algorithm in this study, the optimization objective is adaptation minimization.

Model verification

The residuals and total errors between simulation results and experimental data are calculated as (Cabrera et al.[13]):

$$R\left(y_j\right) = \frac{1}{N}\sum_{i=1}^{N}\left|\tilde{y}_{ij} - y_{ij}\right| \tag{Equation 19}$$

$$J = \frac{1}{M}\sum_{i=1}^{M}E(y_i) \tag{Equation 20}$$

where M denotes the number of variables.

The results pertaining to Participant A Trial 1, which exhibited the best fit (0.12% total error), are presented in Figures 2, 3, 4, 5, 6, and 7. Model verification findings are reported in Table 2, indicating that the error had no significant relationship with the number of strokes or experimental participant. After algorithmic optimization, errors in position and velocity residuals across all three axes were significantly reduced, albeit more so along the X and Y axes, and not to the same extent in the Z direction. The maximum total error observed was 3.99% for Participant B Trial 2, and represented a maximum error reduction of 99.7% in comparison to unoptimized results, specifically observed in Participant B Trial 3.

QUANTIFICATION AND STATISTICAL ANALYSIS

Detailed description of statistical methods is provided in experimental model and study participant details and the method details. The simulation of the model is conducted in MATLAB software environment. The optimization is to reduce the sum of the square percentage errors of the positions in the three directions between the model results and experimental data.

The force parameter settings and the optimized parameters in the GRF model (for one trial) are shown in Tables 3 and 4, respectively. Besides, Table 5 describes statistical analysis method of the COM of the body. And the genetic algorithm parameter settings are provided in Table 6. Finally, the algorithm performance is valued by the total errors, shown in Table 2 along with the participant details.